

DOI: 10.1002/cssc.201402173

# New Hydrogen-Evolution Heteronanostructured Photocatalysts: Pt-Nb<sub>3</sub>O<sub>7</sub>(OH) and Cu-Nb<sub>3</sub>O<sub>7</sub>(OH)

Mohamad Hmadeh,<sup>[a, b]</sup> Veronika Hoepfner,<sup>[a]</sup> Eduardo Larios,<sup>[c, d]</sup> Kristine Liao,<sup>[a]</sup> Jia Jia,<sup>[a]</sup> Miguel Jose-Yacamán,<sup>[c]</sup> and Geoffrey A. Ozin<sup>\*,[a]</sup>

Nanorods of triniobium hydroxide heptaoxide, Nb<sub>3</sub>O<sub>7</sub>(OH), were synthesized by means of a hydrothermal method. Subsequently, Pt and CuO nanoparticles were introduced on the surface of Nb<sub>3</sub>O<sub>7</sub>(OH) nanorods by a microwave-assisted solvothermal nucleation and growth technique. The resulting Pt- and CuO-decorated Nb<sub>3</sub>O<sub>7</sub>(OH) nanorods demonstrated uniform particle dispersion and were fully characterized by X-ray diffraction, electron microscopy, and spectroscopic analysis. Furthermore, the solar-powered photocatalytic hydrogen production properties of these heteronanostructures were studied. The solar-driven H<sub>2</sub> formation rate over Pt-Nb<sub>3</sub>O<sub>7</sub>(OH) was determined to be 710.4 ± 1.7 μmol g<sup>-1</sup> h<sup>-1</sup> with a quantum efficiency of φ = 5.40% at λ = 380 nm. Interestingly, the as-prepared CuO-Nb<sub>3</sub>O<sub>7</sub>(OH) heteronanostructure was found to be inactive under solar irradiation during an induction phase, whereupon it undergoes an in situ photoreduction process to form the photocatalytically active Cu-Nb<sub>3</sub>O<sub>7</sub>(OH). This restructuring process was monitored by an in situ measurement of the time-evolution of the optical absorption spectra. The solar-powered H<sub>2</sub> production for the restructured compound was determined to be 290.3 ± 5.1 μmol g<sup>-1</sup> h<sup>-1</sup>.

Photocatalytic solar fuel production has attracted much attention since Fujishima and Honda's work using the TiO<sub>2</sub> photocatalyst as a photoanode.<sup>[1]</sup> Following this initial discovery, numerous families of semiconductors (e.g. ZnO, ZrO<sub>2</sub>, CdS, ZnS, SiC) have been developed for solar fuel production.<sup>[2]</sup> At pres-

ent, the main obstacle in the development of photocatalytic materials is their low efficiency. Several strategies have been employed in the design of novel materials to enhance the photocatalytic activity.<sup>[3, 4]</sup> The utilization of multi-component nanostructures rather than single semiconductors is one of the most efficient and practical approaches in achieving these highly sought-after characteristics. This is evidenced by semiconductor-based heteronanostructures that have demonstrated charge migration from one component, typically the semiconductor absorbing irradiation, to the other component, which may be a noble metal, a transition metal or metal oxide, a metal sulfide, or another semiconductor with proper band-edge positions.<sup>[3-5]</sup> Because the Fermi energy levels of the noble and coinage metals such as Pt, Rh, Pd, Ru, Cu, Ag, and Au are typically lower than those of semiconductors, the metal nanoparticles can act as electron sinks, facilitating interfacial electron transfer and ultimately decreasing the electron-hole recombination rate as well as creating a new catalytic site for the reduction.<sup>[5, 6]</sup> Although titania is the most commonly studied photocatalyst, a series of niobium-based semiconductors (e.g. HNb<sub>3</sub>O<sub>8</sub>, HNbO<sub>3</sub>, H<sub>4</sub>Nb<sub>2</sub>O<sub>7</sub>, H<sub>4</sub>Nb<sub>6</sub>O<sub>17</sub>) have attracted much attention recently due to their favorable properties such as high stability under light irradiation, chemical inertness, and non-toxicity.<sup>[7]</sup> Furthermore, it is believed that the protonic acidity in these semiconductors can promote adsorption of water, CO<sub>2</sub>, and some organic molecules.<sup>[7]</sup> Even though Nb<sub>3</sub>O<sub>7</sub>(OH) materials have been reported as photocatalysts used in dye degradation and dye-sensitized solar cells, the photocatalytic properties of Nb<sub>3</sub>O<sub>7</sub>(OH) nanorods and their heteronanostructures towards hydrogen evolution remain unexplored.<sup>[8]</sup>

By combining the favorable properties of triniobium hydroxide heptaoxide, Nb<sub>3</sub>O<sub>7</sub>(OH), with the advantages associated with metal-semiconductor heteronanostructures, a novel and highly efficient photocatalyst can be created. Herein, the synthesis and characterization of Nb<sub>3</sub>O<sub>7</sub>(OH) nanorods as well as their Pt- and CuO-decorated heteronanostructures are reported. The photocatalytic hydrogen production properties of the pure Nb<sub>3</sub>O<sub>7</sub>(OH) nanorods and of the heteronanostructures (Pt-Nb<sub>3</sub>O<sub>7</sub>(OH) and CuO-Nb<sub>3</sub>O<sub>7</sub>(OH)) are investigated.

Nanocrystals of Nb<sub>3</sub>O<sub>7</sub>(OH) were prepared via a hydrothermal method (see Experimental Section for more details). The powder X-ray diffraction (PXRD) pattern of the as-synthesized compound (Figure 1 A) was indexed as an orthorhombic structure with lattice parameters of *a* = 20.74 Å, *b* = 3.82 Å and *c* = 3.93 Å (PDF, file No.: 00-031-0928) and no additional peaks were observed. The Nb<sub>3</sub>O<sub>7</sub>(OH) crystal structure is constructed

[a] Dr. M. Hmadeh,<sup>\*</sup> Dr. V. Hoepfner,<sup>\*</sup> Dr. K. Liao, J. Jia, Prof. G. A. Ozin  
Materials Chemistry Research Group  
Department of Chemistry  
University of Toronto  
80 St. George Street, Toronto, Ontario M5S 3H6 (Canada)  
E-mail: gozin@chem.utoronto.ca

[b] Dr. M. Hmadeh<sup>\*</sup>  
Department of Chemistry  
American University of Beirut  
Beirut 11-0236 (Lebanon)

[c] E. Larios, Prof. M. Jose-Yacamán  
Physics Department  
University of Texas at San Antonio  
One UTSA Circle, San Antonio, TX 78249 (USA)

[d] E. Larios  
Departamento de Ingeniería Química  
Universidad de Sonora  
83000 Hermosillo, Sonora (México)

[\*] These authors contributed equally to this work.

Supporting Information for this article is available on the WWW under <http://dx.doi.org/10.1002/cssc.201402173>.

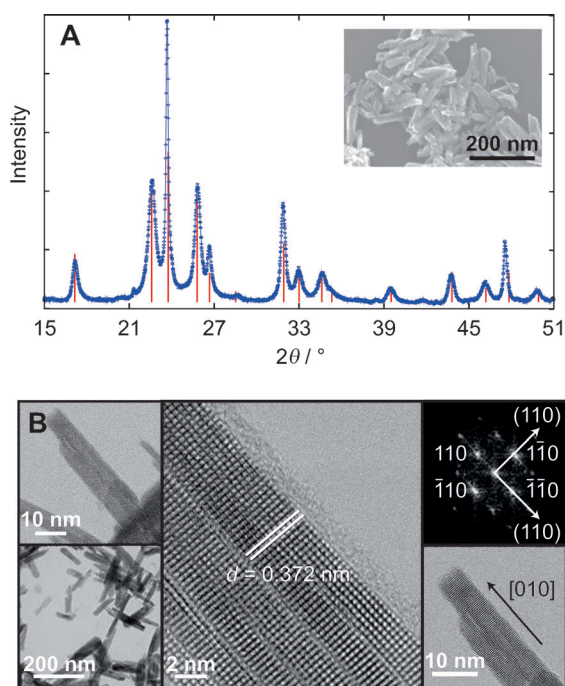


**Figure 1.** A) Powder X-ray diffraction pattern (blue) of the as synthesized  $\text{Nb}_3\text{O}_7(\text{OH})$  crystals compared to the simulated pattern (red bars). Inset: SEM image of the as-synthesized  $\text{Nb}_3\text{O}_7(\text{OH})$ . B) HRTEM images and FFT calculations of  $\text{Nb}_3\text{O}_7(\text{OH})$  nanorods.

from octahedral building blocks that resemble the well-known  $\text{ReO}_3$ -type structure with a crystallographic shear in one dimension (Figure S1).<sup>[9]</sup> The morphology of the sample was analyzed by HRSEM and HRTEM. The obtained micrographs of the as-synthesized  $\text{Nb}_3\text{O}_7(\text{OH})$  are shown in Figure 1B and display uniform nanorod shape with an average diameter of 20 nm and an average length of 100 nm. Fast Fourier transform (FFT) analysis was performed on the HRTEM micrographs. The FFT analysis clearly demonstrates the highly crystalline nature of the as-synthesized  $\text{Nb}_3\text{O}_7(\text{OH})$  nanorods and confirms the fringe spacings of 0.372 nm and 1.04 nm, which are consistent with the  $d$ -values of the (110) and (200) reflection planes of the orthorhombic  $\text{Nb}_3\text{O}_7(\text{OH})$ , respectively (Figure 1B and Figure S2).<sup>[9]</sup> It has been shown that the photocatalytic activity depends on the specific surface area of the catalyst,<sup>[10]</sup> with a high surface area affording a material with a greater number of reaction sites and thus the BET surface area of the  $\text{Nb}_3\text{O}_7(\text{OH})$  nanorods was measured and found to be  $120 \text{ m}^2 \text{ g}^{-1}$ .

To study the structural and electronic properties of the  $\text{Nb}_3\text{O}_7(\text{OH})$  nanorods, X-ray photoelectron spectroscopy (XPS) measurements were carried out. The Nb 3d and O 1s core level spectra are shown in Figure S4. The core level peaks of Nb  $3d_{5/2}$  and Nb  $3d_{3/2}$  are located at 207.74 eV and 210.50 eV respectively. The O 1s core level peak can be de-convoluted into two individual peaks, a main peak at 530.8 eV due to the oxygen anions ( $\text{O}^{2-}$ ) bound to the niobium, and a lesser peak at 531.8 eV due to the presence of OH

groups (Figure S4).<sup>[8]</sup> From the XPS measurements, the energies of the valence band maximum (VBM) and work function (and consequently, the Fermi level) of our material with respect to the vacuum level were evaluated to be  $-7.74 \text{ eV}$  and  $-4.25 \text{ eV}$ , respectively (Figure S4). The optical absorption of as-prepared  $\text{Nb}_3\text{O}_7(\text{OH})$  nanorods was measured by UV/Vis absorption spectroscopy in the range of 250–900 nm (Figure S4). The spectrum displays an absorption edge at 330 nm, which led to the estimation of the electronic energy band-gap value to be 3.85 eV. By combining this result with the XPS data, the conduction band (CB) edge potential of this material was determined ( $E_{\text{CB}} = E_{\text{VB}} + E_{\text{g}}$ ) and shown in Figure S5.

The obtained band energy levels are found to be suitable for photocatalytic water splitting as the valence band maximum and the conduction band minimum are located at the desirable potential energies. This result prompted the study of the compound's photocatalytic properties. To this end, pure  $\text{Nb}_3\text{O}_7(\text{OH})$  was tested under aqueous conditions in the presence of 25 vol% methanol as a hole scavenger and no hydrogen formation was observed. Nevertheless a color change was observed and the white dispersion turned dark blue during light exposure (Figure 2A). A similar photochromic phenomenon is well-known in titania and was among the first examples for the photoreactivity of  $\text{TiO}_2$ , which was found to turn gray-blue followed by dark blue in the presence of glycerol and under light irradiation.<sup>[11]</sup> In this early study, the color change was ascribed to a reduction of the material. Furthermore, in a more recent study, the blue color of reduced titania was attributed to IR absorption resulting from (i) direct optical transition of electrons from trap states ( $\text{Ti}^{3+}$ ) into the conduction band and (ii) intra-CB transitions of thermally excited electrons in the CB.<sup>[12]</sup> The color change of  $\text{Nb}_3\text{O}_7(\text{OH})$  was monitored by the change in the absorption spectra of the photocatalyst dispersion (Figure S10). As a result, two different effects were noted: (i) an increase in absorption approaching the IR region

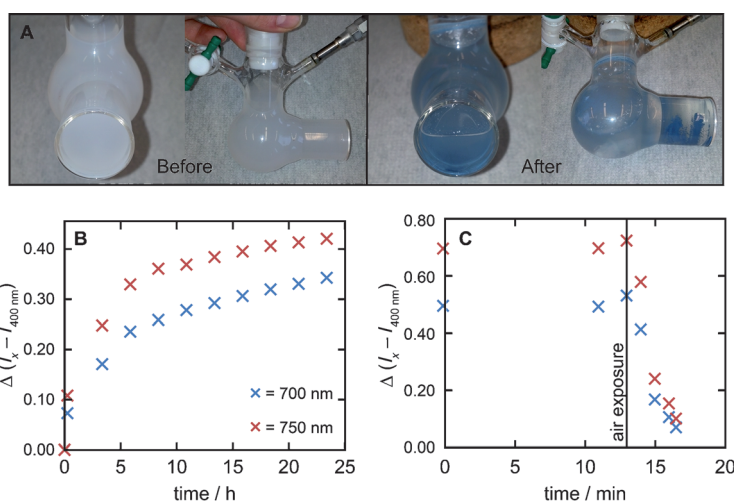


**Figure 2.** A) Visual comparison of the  $\text{Nb}_3\text{O}_7(\text{OH})$  dispersion before and after solar irradiation. B) Color change was monitored by the difference  $\Delta(I_x - I_{400 \text{ nm}})$  with  $x = 700 \text{ nm}$  (x) and  $750 \text{ nm}$  (x) during solar illumination of  $\text{Nb}_3\text{O}_7(\text{OH})$  in the presence of MeOH. C) Re-oxidation of the  $\text{Nb}_3\text{O}_7(\text{OH})$  surface under air exposure.

and (ii) a baseline decrease during the experiment (Figure S10). Though the increased IR absorption explains the color change, the decrease is most likely associated with aggregation and sedimentation of the dispersed catalyst over time. To explain these two conflicting effects, the relative differences in absorption intensity are calculated—this can be considered as a baseline correction—and plotted against the illumination time in Figure 2B. From this representation it can be seen that the color change occurs in the first 5 h of irradiation and stabilizes afterwards. On the other hand, as soon as the photocatalyst dispersion is exposed to air and thus to  $O_2$  the blue color disappears within minutes (Figure 2C).

Based on these observations, a mechanism of similar origin to that used to explain the color change observed for  $TiO_2$  seems plausible and is illustrated in Figure 4. Under light illumination, electrons and holes are generated on  $Nb_3O_7(OH)$ . While the holes are scavenged by MeOH, the electrons remain in  $Nb^{4+}$  trap states and/or the conduction band, giving rise to an increased absorption in the IR region, likely from inter-valence charge-transfer, resulting in a reduced surface of the photocatalyst. The reduced catalyst surface is stable under inert conditions, but re-oxidizes easily in the presence of an oxidizing agent, that is,  $O_2$ . Because no hydrogen formation is observed, it can be concluded that the reduction of protons is kinetically hindered on the surface of  $Nb_3O_7(OH)$  as it should be feasible from a pure thermodynamic point of view based on the CB edge alignment. In order to overcome the reduction kinetic barrier, heteronanostructures of Pt- $Nb_3O_7(OH)$  and CuO- $Nb_3O_7(OH)$  were prepared. Based on the band energies and alignment, the Pt or CuO nanoparticles of the heteronanostructure can act as a sink for photo-generated electrons and function as the catalytic site for proton reduction.

The Pt nanoparticles have previously been prepared through several methods.<sup>[6, 13]</sup> One such method—the energy-efficient microwave-assisted synthesis—is well known for its facile preparation of simple metallic nanostructured materials. However, there are relatively few examples of this method employed in the synthesis of supported metal particles.<sup>[14]</sup> To prepare Pt- $Nb_3O_7(OH)$  and CuO- $Nb_3O_7(OH)$  heteronanostructures, a microwave-assisted solvothermal technique using ethanol as a reducing agent was successfully performed (see experimental section for more details). HRTEM images of the resulting Pt- $Nb_3O_7(OH)$  and CuO- $Nb_3O_7(OH)$  heteronanostructures are shown

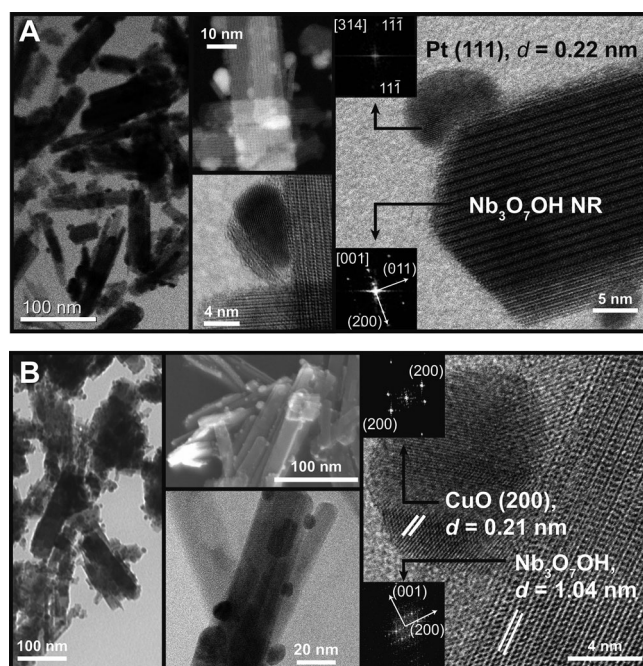


**Figure 3.** HRTEM images and FFT calculations of A) Pt-decorated  $Nb_3O_7(OH)$  and B) CuO-decorated  $Nb_3O_7(OH)$  nanorods.

in Figure 3. The Pt nanoparticles were found to be single crystals and well dispersed on the surface with a diameter of 2–7 nm (Figure S5). The HRTEM images show atomic planes with a spacing of 0.22 nm for the nanoparticles (Figure 3A), which

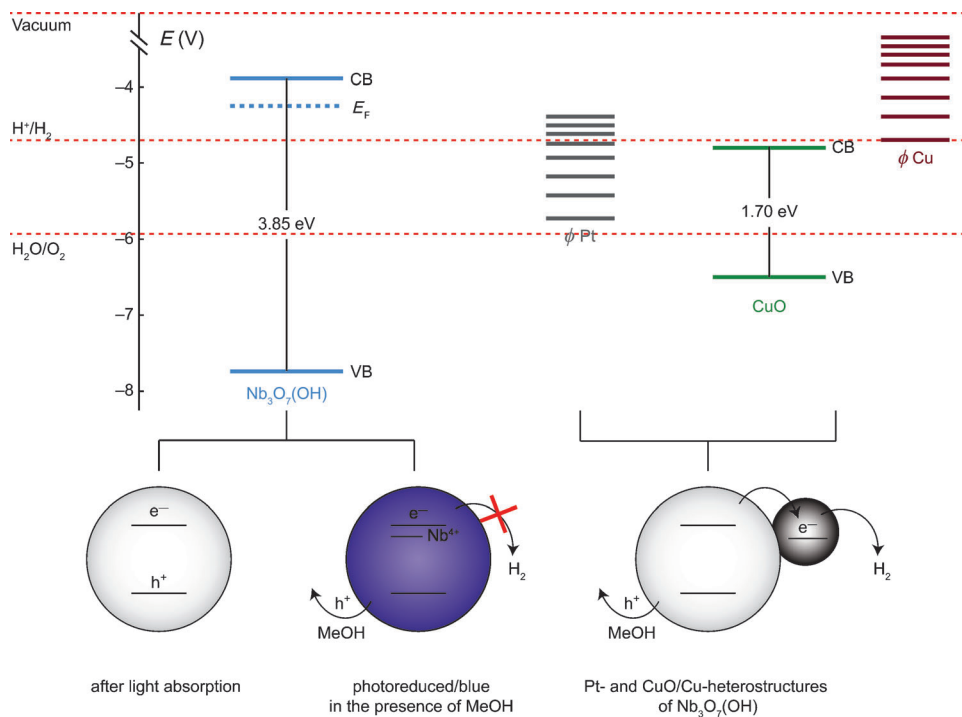


**Figure 4.** Band energy diagram of  $Nb_3O_7(OH)$  and proposed mechanism: Electrons and holes are generated in white  $Nb_3O_7(OH)$  under light illumination. Holes are scavenged by methanol while the reduction of protons is kinetically hindered, which leads to a reduced, blue form of  $Nb_3O_7(OH)$ . To overcome the kinetic barrier, the surface of the photocatalyst is decorated with a second component (Pt or CuO/Cu).

can be ascribed to the (111) reflection plane of bulk platinum. This indicates that, in this case, nanoparticles have the same structure as that of the bulk material. Representative images recorded for copper-oxide-decorated  $\text{Nb}_3\text{O}_7(\text{OH})$  are shown in Figure 3B. Again, the supported nanoparticles are highly crystalline with an average size of 5–10 nm. The atomic planes were observed with a spacing of 0.211 nm (Figure 3B and S6), which could be ascribed to the (200) reflection plane of  $\text{Cu}_2\text{O}$  or  $\text{CuO}$ .

The chemical states of platinum and copper oxide in the heteronanostructure samples were further characterized by PXRD and XPS. In the powder XRD diffraction patterns, the diffraction peaks ascribed to  $\text{Nb}_3\text{O}_7(\text{OH})$  were the only peaks present for each sample (Figure S7). Due to low metal loading and the small diameter of the nanoparticles, no PXRD reflections associated with platinum or copper oxide were observed. However, shifts in the positions of some peaks were observed, which indicate slight modification in the unit cell parameters. XPS measurements, on the other hand, were able to detect the low metal loading. The binding energy of Pt  $4f_{7/2}$  was found to be 70.9 eV for the Pt- $\text{Nb}_3\text{O}_7(\text{OH})$ , confirming that Pt was in the metallic state in the sample (Figure S8). Although the Cu  $2p_{3/2}$  XPS spectrum shows a broad and low intensity peak around 934.2 eV, a satellite peak which is characteristic of  $\text{CuO}$  can be clearly observed (see Figure S8). XPS is a surface-sensitive technique; thus only  $\text{CuO}$  is present on the surface region of the as-synthesized copper-oxide-decorated  $\text{Nb}_3\text{O}_7(\text{OH})$  sample. The Pt and Cu content (wt%) in the as-synthesized Pt- $\text{Nb}_3\text{O}_7(\text{OH})$  and  $\text{CuO-Nb}_3\text{O}_7(\text{OH})$  heteronanostructures were evaluated by inductively coupled plasma–atomic emission (ICP–AES) analysis and was found to be 0.5 wt% and 15 wt%, respectively.

The photocatalytic activity of the as-synthesized heteronanostructures was evaluated under the same conditions employed for the pure  $\text{Nb}_3\text{O}_7(\text{OH})$  nanorods. Starting with the Pt-decorated samples, one can see that the concept of introducing a nanoparticle enabled the material to overcome the kinetic barrier. In contrast to Pt- $\text{TiO}_2$  heterostructures the introduction of Pt onto  $\text{Nb}_3\text{O}_7(\text{OH})$  nanorods is necessary to induce the hydrogen evolution reaction in the first place and is not only a tool for increasing the performance of the catalysts. Figure 5 shows the hydrogen-formation rate of Pt- $\text{Nb}_3\text{O}_7(\text{OH})$  under Xe lamp illumination. Up to four formation cycles were performed in the course of about 26 h and the reactor was purged with  $\text{N}_2$  before each cycle. The same linear  $\text{H}_2$  formation rates were obtained in all cases, indicating the catalyst is stable against decomposition or deactivation. The last two cycles shown in Figure 5 were performed with an AM 1.5 filter, which simulates the direct solar spectrum when the sun is at a zenith angle of  $48.2^\circ$ . Even though the formation rate is lower, the catalyst is still active and continues to produce  $\text{H}_2$  under direct solar illumination.

To gain a better understanding of the performance of Pt-decorated  $\text{Nb}_3\text{O}_7(\text{OH})$ , the quantum efficiencies (QE) were calculated for different light intensities and spectral distributions. The results are summarized in Table 1 and a detailed description of the calculation is found in the Supporting Information.

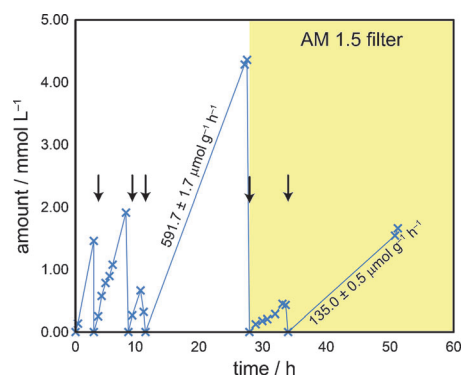


**Figure 5.** Hydrogen formation from Pt-decorated  $\text{Nb}_3\text{O}_7(\text{OH})$  under solar irradiation (120 W Xe lamp) in the presence of 25 vol% MeOH. Black arrows indicate a purge of the reactor with nitrogen to remove all hydrogen and start a new formation cycle. In the yellow region, an AM 1.5 filter is applied.

**Table 1.** Overview of the different photocatalytic testing conditions and the corresponding quantum efficiency ( $\phi$ ) for the Pt-decorated triniobium hydroxide heptaoxide (Pt- $\text{Nb}_3\text{O}_7(\text{OH})$ ).

Lamp	$I$ ( $h\nu$ ) [ $\text{W m}^{-2}$ ]	Filter	Formation rate [ $\mu\text{mol g}^{-1} \text{h}^{-1}$ ]	$\phi$ [%]
120 W	2670	none	$591.7 \pm 1.7$	0.08
120 W	1500	AM 1.5	$135.0 \pm 0.5$	0.03
300 W	5600	AM 1.5	$710.4 \pm 1.7$	0.03
300 W	220	380 band pass	$32.8 \pm 1.9$	5.40

Using the same 120 W Xe lamp, the QE (from 0.08% to 0.03%) as well as the formation rate (from 592 to  $135 \mu\text{mol g}^{-1} \text{h}^{-1}$ ) decreases on applying the AM 1.5 filter and thus changing the spectral distribution. This can easily be understood since the filter decreases the high-energy UV light intensity. On the other hand, if the light intensity is increased (120 W vs. 300 W Xe lamp) while keeping the spectral distribution constant (AM 1.5 filter in both cases), the formation rate increases (from 135 to  $710 \mu\text{mol g}^{-1} \text{h}^{-1}$ ) but the quantum efficiency remains constant at  $\phi = 0.03\%$ . Since the QE relates the formation rate to the light intensity, the constant QE indicates a linear trend between both. In all cases the quantum efficiencies are relatively low since a large amount of visible light is not absorbed by the photocatalyst. To evaluate the performance of the catalyst at a wavelength of relatively good absorption but still using the higher intensity range of the solar irradiation, a 380 nm band pass filter was employed, resulting in a quantum efficiency of  $\phi_{380 \text{ nm}} = 5.40\%$ . This is competitive with the performances of other photocatalysts in the presence of an organic hole scavenger [e.g. Pt- $\text{TiO}_2$  with polyvinyl alcohol ( $\phi_{380 \text{ nm}} = 0.35\%$ ) and with sugar ( $\phi_{380 \text{ nm}} = 7.08\%$ ); Pt/ $\text{H}_2\text{LaNb}_2\text{O}_7:\text{In}$  with methanol ( $\phi_{>290 \text{ nm}} = 1.54\%$ ), and Pt- $\text{TiO}_2$  with ethanol ( $\phi_{\text{UV light}} \approx 10\%$ )].<sup>[15]</sup>

Based on the success of the Pt-decorated catalyst, the  $\text{CuO}$ -decorated catalyst was tested and the results using this heteronanostructure are summarized in Figure 6. Interestingly, no hydrogen evolution was observed during the first 4 h of irradiation, but a noticeable color change from greenish to violet-red

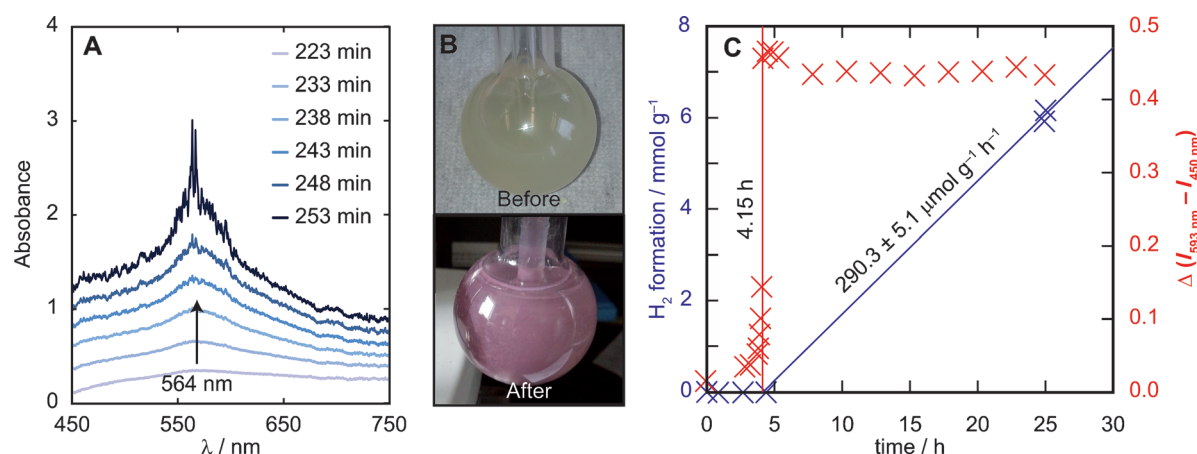


**Figure 6.** A) In situ photoreduction of CuO followed by the formation of an absorption band centered at 564 nm which corresponds to the Cu plasmon resonance. B) The color of the CuO-Nb<sub>3</sub>O<sub>7</sub>(OH) dispersion before and after 4 h of irradiation. C) Hydrogen formation and color change monitored over time.

was observed (Figure 6B) while a new peak centered at 564 nm evolved in the absorption spectra of the dispersion (Figure 6A). Indeed, the surface plasmon resonance of Cu has been reported to be 573 nm for Cu films as well as 564 nm and 570 nm for Cu nanowires with a diameter of 20 nm (calculated and experimental values, respectively).<sup>[16]</sup> Based on the band energy diagrams of Nb<sub>3</sub>O<sub>7</sub>(OH), CuO, and Cu, we strongly believe that the photogenerated electrons on the surface of Nb<sub>3</sub>O<sub>7</sub>(OH) first reduce CuO to form Cu particles. The in situ-generated Cu-Nb<sub>3</sub>O<sub>7</sub>(OH) now serves as the photocatalytic active system similar to Pt-decorated Nb<sub>3</sub>O<sub>7</sub>(OH) and—if the time of the color change is taken as a start of the photocatalytic reaction—a formation rate of  $290.3 \pm 5.1 \mu\text{mol g}^{-1} \text{h}^{-1}$  is obtained (Figure 6C). As soon as the violet-red solution is exposed to air, the color change is reversed and a greenish solution is obtained, making it impossible to further characterize the reduced system. It should be noted that the photoactive system, Cu-Nb<sub>3</sub>O<sub>7</sub>(OH), itself is stable under photocatalytic reaction conditions making Cu-Nb<sub>3</sub>O<sub>7</sub>(OH) a good photocatalyst even though it is not stable under ambient conditions. TEM images of the catalyst system after solar irradiation indicate that larger CuO particles had separated from Nb<sub>3</sub>O<sub>7</sub>(OH), while smaller particles were still attached and thus the heteronanostructure is not completely lost during the structural changes on CuO (Figure S9). A similar in situ restructuring process has been recently demonstrated for the CuO-TiO<sub>2</sub> system.<sup>[17]</sup> In this heteronanostructure, the non-active CuO-TiO<sub>2</sub> undergoes a reduction reaction under solar light irradiation to form the active Cu<sub>2</sub>O-TiO<sub>2</sub>. The CB of TiO<sub>2</sub> is located at an energy potential higher than that of CuO but lower than that of Cu<sub>2</sub>O. However, the CB level of Nb<sub>3</sub>O<sub>7</sub>(OH) is higher than that of both copper oxides (Cu<sub>2</sub>O and CuO). Therefore, the Nb 3d electrons are able to reduce the copper oxides to produce the Cu-decorated Nb<sub>3</sub>O<sub>7</sub>(OH) which is the active species.

In conclusion, single-crystal Nb<sub>3</sub>O<sub>7</sub>(OH) nanorods of high surface area have been successfully synthesized by means of a facile hydrothermal method. The nanorods were subsequently decorated with platinum and copper oxide nanoparticles using a microwave-assisted solvothermal nucleation and

growth technique to produce Pt-Nb<sub>3</sub>O<sub>7</sub>(OH) and CuO-Nb<sub>3</sub>O<sub>7</sub>(OH) heteronanostructures. Furthermore, the photocatalytic properties of the developed nanostructures for H<sub>2</sub> production were investigated and a mechanism of the photocatalytic reaction was proposed. Our studies demonstrate the importance of the design of heteronanostructures in overcoming the kinetic barriers to hydrogen production and, therefore, enhancing photocatalytic activity.

## Experimental Section

**Synthesis:** In a typical procedure for synthesis of Nb<sub>3</sub>O<sub>7</sub>(OH) nanorods, niobium powder (1 g, Nb (s) 325 Mesh, Aldrich) was ultrasonically dissolved in hydrochloric acid solution (50 mL, 2–8 M; HCl, Sigma-Aldrich) contained in a pyrex beaker. After stirring for 15 min, the solution was placed into a Teflon-lined stainless steel autoclave of 100 mL capacity. The hydrothermal reaction was performed at  $T = 200^\circ\text{C}$  for 12 h and subsequently naturally cooled to room temperature. The as-prepared product was washed three times with deionized water and ethanol. Finally, the sample was dried in a vacuum oven at  $T = 70^\circ\text{C}$  for 5 h.

The Pt-Nb<sub>3</sub>O<sub>7</sub>(OH) heterostructure was synthesized via a microwave-assisted reaction, typically, 100 mg of Nb<sub>3</sub>O<sub>7</sub>(OH) were suspended in anhydrous ethanol (20 mL) in a pyrex vessel of 40 mL capacity. H<sub>2</sub>PtCl<sub>6</sub> solution (40  $\mu\text{L}$ , 0.02 M) was added to the dispersion under sonication. After 30 min of sonication, the vessel was capped and transferred to the microwave reactor (CEM Discover, 250 W, 250 psi,  $T = 150^\circ\text{C}$ , 10 min). After filtration and washing with ethanol, the resultant heteronanostructure of Pt-Nb<sub>3</sub>O<sub>7</sub>(OH) was dried in a vacuum oven at  $T = 70^\circ\text{C}$  for 5 h. The CuO-Nb<sub>3</sub>O<sub>7</sub>(OH) heteronanostructure was synthesized under the same conditions using 0.3 mmol of Cu(OAc)<sub>2</sub> as a copper source.

**Photocatalytic tests:** All photocatalytic tests were performed in a home built, gas-tight pyrex reactor with a quartz window. The photocatalyst powder (1 g L<sup>-1</sup>) was dispersed in distilled water and methanol (25 vol%, HPLC grade). Prior to each run, the reactor was purged with nitrogen for 20 min and the first sample was taken before the photocatalytic reaction was started. A Newport 120 W or 300 W Xe lamp was used for solar irradiation and an air mass (AM) 1.5 filter (Newport) was applied to simulate the direct solar spectrum when the sun is at a zenith angle of 48.2°. To test the long-term stability of the photocatalyst and the reproducibility of

the H<sub>2</sub> formation, the reactor was purged after a few hours to remove all products and start a new formation cycle.

Gas samples were extracted with a gas-tight syringe, separated by gas chromatography (GC, Agilent 7820A GC) and detected by a thermal conductivity detector (TCD). A 1.5 m Molesieve 13 X column (80–100 mesh) was used for the separation of H<sub>2</sub>, O<sub>2</sub>, and N<sub>2</sub>, and an integrated 1 m Haysep Q column (80–100 mesh) was used to first separate CO<sub>2</sub> and water vapor to avoid the contamination of the Molesieve column.

An Ocean Optic SD2000 fiber optic spectrometer was used for in situ measurements of the relative absorption spectra of the dispersion. The spectrum at  $t=0$  min was used as a reference for all other collected spectra.

## Acknowledgements

We are deeply indebted to the Ontario Ministry of Economic Development and Innovation (MEDI) for strong and sustained financial support of the University of Toronto Solar Fuels Project. We would like to acknowledge the NSF for support with grants DMR-1103730, "Alloys at the Nanoscale and PREM NSF PREM Grant # DMR 0934218; We also acknowledge the grants from the National Center for Research Resources (5 G12RR013646-12) and the National Institute on Minority Health and Health Disparities (G12MD007591) from the National Institutes of Health. "We gratefully thank Dr. Paul O'Brien (Chemical Engineering and Applied Chemistry at the University of Toronto), Dr. Benoit Mahler and Mrs. Laura Hoch (department of Chemistry at University of Toronto) for experimental assistance and invaluable discussions.

**Keywords:** heteronanostructure • hydrogen production • photocatalysis • triniobium hydroxide heptaoxide

- [1] A. Fujishima, K. Honda, *Nature* **1972**, *238*, 37–38.
- [2] a) T. Inoue, A. Fujishima, S. Konishi, K. Honda, *Nature* **1979**, *277*, 637–638; b) K. Sayama, H. Arakawa, *J. Phys. Chem.* **1993**, *97*, 531–533; c) Z. R. Tian, J. A. Voigt, J. Liu, B. McKenzie, M. J. Mcdermott, M. A. Rodriguez, H. Konishi, H. Xu, *Nat. Mater.* **2003**, *2*, 821–826; d) H. Zhou, Y. Qu, T. Zeid, X. Duan, *Energy Environ. Sci.* **2012**, *5*, 6732–6743; e) S. N. Habisreutinger, L. Schmidt-Mende, J. K. Stolarczyk, *Angew. Chem. Int. Ed.* **2013**, *52*, 7372–7408; *Angew. Chem.* **2013**, *125*, 7516–7557.
- [3] a) A. L. Linsebigler, G. Q. Lu, J. T. Yates, *Chem. Rev.* **1995**, *95*, 735–758; b) H. Tong, S. Ouyang, Y. Bi, N. Umezawa, M. Oshikiri, J. Ye, *Adv. Mater.* **2012**, *24*, 229–251; c) W. Fan, Q. Zhang, Y. Wang, *Phys. Chem. Chem. Phys.* **2013**, *15*, 2632–2649; d) I. E. Wachs, S. P. Phivilay, C. A. Roberts, *ACS Catal.* **2013**, *3*, 2606–2611.
- [4] a) G. Liu, L. Wang, H. Yang, H. Cheng, G. Lu, *J. Mater. Chem.* **2010**, *20*, 831–843; b) L. Jing, W. Zhou, G. Tian, H. Fu, *Chem. Soc. Rev.* **2013**, *42*, 9509–9549.
- [5] a) B. Kraeutler, A. J. Bard, *J. Am. Chem. Soc.* **1978**, *100*, 4317–4318; b) S. Kim, W. Choi, *J. Phys. Chem. B* **2002**, *106*, 13311–13317; c) W. N. Wang, J. W. An, B. Ramalingam, S. Mukherjee, D. M. Niedzwiedzki, S. Gangopadhyay, P. Biswas, *J. Am. Chem. Soc.* **2012**, *134*, 11276–11281; d) S. I. In, D. D. Vaughn II., R. E. Schaak, *Angew. Chem.* **2012**, *124*, 3981–3984; e) S. Xie, Y. Wang, Q. Zhang, W. Fan, W. Deng, Y. Wang, *Chem. Commun.* **2013**, *49*, 2451–2453; f) A. Tanaka, K. Nakanishi, R. Hamada, K. Hashimoto, H. Kominami, *ACS Catal.* **2013**, *3*, 1886–1891.
- [6] S. T. Kochuveedu, Y. H. Jang, D. H. Kim, *Chem. Soc. Rev.* **2013**, *42*, 8467–8493.
- [7] a) X. K. Li, N. Kikugawa, J. H. Ye, *Adv. Mater.* **2008**, *20*, 3816–3819; b) A. Kudo, H. Kato, S. Nakagawa, *J. Phys. Chem. B* **2000**, *104*, 571–575; c) S. Liang, L. Wen, S. Lin, J. Bi, P. Feng, X. Fu, L. Wu, *Angew. Chem. Int. Ed.* **2014**, *53*, 2951–2951; *Angew. Chem.* **2014**, *126*, 2995–2999; d) S. Liang, X. Wang, Y. Chen, J. Zhu, Y. Zhang, X. Wang, Z. Li, L. Wu, *Nanoscale* **2010**, *2*, 2262–2268.
- [8] a) J. Wu, J. Wang, H. Li, D. Xue, *Thin Solid Films* **2013**, *544*, 545–550; b) H. Zhang, Y. Wang, D. Yang, Y. Li, H. Liu, P. Liu, B. J. Wood, H. Zhao, *Adv. Mater.* **2012**, *24*, 1598–1603.
- [9] F. Izumi, H. Kodama, *Z. Anorg. Allg. Chem.* **1978**, *441*, 196–204.
- [10] a) J. G. Yu, Y. R. Su, B. Cheng, *Adv. Funct. Mater.* **2007**, *17*, 1984–1990; b) X. F. Chen, X. C. Wang, X. Z. Fu, *Energy Environ. Sci.* **2009**, *2*, 872–877; c) X. Jiang, T. Wang, *Environ. Sci. Technol.* **2007**, *41*, 4441–4446.
- [11] C. Renz, *Helv. Chim. Acta* **1921**, *4*, 961–968.
- [12] a) T. Berger, *J. Phys. Chem. B* **2005**, *109*, 6061–6068; b) M. Takeuchi, G. Martra, S. Coluccia, M. Anpo, *J. Phys. Chem. C* **2007**, *111*, 9811–9817.
- [13] a) M. Sadeghi, W. Liu, T. G. Zhang, P. Stavropoulos, B. Levy, *J. Phys. Chem.* **1996**, *100*, 19466–19474; b) J. He, I. Ichinose, T. Kunitake, A. Nakao, *Langmuir* **2002**, *18*, 10005–10010; c) T. J. Hsueh, S. J. Chang, C. L. Hsu, Y. R. Lin, I. C. Chen, *Appl. Phys. Lett.* **2007**, *91*, 053111–053113; d) P. A. K. Seibold, A. J. McEvoy, J. Kiwi, *J. Phys. Chem.* **1989**, *93*, 1510–1515;
- [14] a) M. Tsuji, M. Hashimoto, Y. Nishizawa, M. Kubokawa, T. Tsuji, *Chem. Eur. J.* **2005**, *11*, 440–452; b) X. Yan, H. Liu, K. Y. Liew, *J. Mater. Chem.* **2001**, *11*, 3387–3391; c) S. Kundu, K. Wang, H. Liang, *J. Phys. Chem. C* **2009**, *113*, 5157–5161; d) Z. L. Liu, J. Y. Lee, W. X. Chen, M. Han, L. M. Gan, *Langmuir* **2004**, *20*, 181–187; e) K. Fuku, T. Kamegawa, K. Mori, H. Yamashita, *Chem. Asian J.* **2012**, *7*, 1366–1371.
- [15] a) T. Kawai, T. Sakata, *Chem. Lett.* **1981**, 81–84; b) Y. Wei, J. Li, Y. Huang, M. Huang, J. Lin, J. Wu, *Sol. Energy Mater. Sol. Cells* **2009**, *93*, 1176–1181; c) Y. Yang, C. Chang, H. Idriss, *Appl. Catal. B* **2006**, *67*, 217–222.
- [16] a) J. L. Duan, T. W. Cornelius, J. Liu, S. Karim, H. J. Yao, O. Picht, M. Rauber, S. Müller, R. Neumann, *J. Phys. Chem. C* **2009**, *113*, 13583–13587; b) P. F. Robusto, R. Braunstein, *Phys. Status Solidi* **1981**, *107*, 443–449.
- [17] Z. Wang, Y. Liu, D. J. Martin, W. Wang, J. Tang, W. Huang, *Phys. Chem. Chem. Phys.* **2013**, *15*, 14956–14960.

Received: March 13, 2014

Published online on June 18, 2014